34th EPS Conference on Plasma Phys. Warsaw, 2 - 6 July 2007 ECA Vol.**31F**, P-2.017 (2007)

ELM divertor heat load in forward and reversed field in ASDEX Upgrade

T.Eich, A. Kallenbach, A.Herrmann, J.C.Fuchs, C.S.Chang[1], D. Tskhakaya[2]
and the ASDEX Upgrade Team
Max-Planck-Institut für Plasmaphysik, EURATOM Association, Garching, Germany
[1] *Courant Institute of Mathematical Sciences, New York University, U.S.A.*
[2] *Association-ÖAW, Institute of Theoretical Physics, A-6020 Innsbruck Austria*

Introduction

H-mode plasmas develop a pronounced edge transport barrier and steep edge gradients driving quasi-periodic barrier relaxations known as Edge Localised Modes (ELMs). Type-I ELMs impose a sudden release of energy from the pedestal region, from which the largest fraction is transported along field lines to the divertor region. Scaling of ELM losses and heat load from present devices show that the divertor life time in ITER will be limited due to ELMs [1].

Although good progress was achieved in recent years for ELM characterisation, still the observation of the larger fraction to be deposited on the inboard divertor in normal field direction (ion $\vec{B} \times \nabla B$ drift direction points towards the (active) X-point) and the larger fraction deposited on the outer divertor in reversed field (ion $\vec{B} \times \nabla B$ drift direction points away from the (active) X-point) is not understood [2]. For ASDEX Upgrade discharges in Upper Single Null (USN) geometry with both field directions, it has been shown that an excess amount of positive charges is measured on the target side receiving the larger ELM energy load [2] and roughly the same amount of negative charges on the other target. The latter observation led to the conclusion that thermoelectric currents cannot explain the observed asymmetry, since the higher power load is observed at the cold electron side of the SOL [2]. Beside other possible explanations, two mechanism have been recently proposed to explain the latter effect:

First, an increase of the sheath potential at the cold electron side due to a change of the edge current distribution during an ELM locally accelerating ions in front of the target plates [3]. Since for the performed USN discharges in ASDEX Upgrade no probe data are available, a comparison of the ELM power load measured by infra red (IR) and Langmuir probes (LP) is performed [3] for Lower Single Null (LSN) geometry in normal field and reveals that the required potential increase at the ion side is considerably larger than the measured (highly fluctuating) potential increase [3].

Second, direct ion orbit losses from the pedestal region during the ELM will preferentially hit the inner target plate in normal field and the outer target plate in reversed field [4] if the typical ion energy is below the potential hill associated with the radial electric field commonly observed in H-Mode plasmas under the assumption that a non-negligible fraction of the H-mode potential hill survives during the most violent starting phase of the nonlinear ELM activities. In the model proposed in [4] a random walk process due to ergodization during the ELM event moves the ions radially outward. The potential hill has typically values of about 1keV in ASDEX Upgrade [5] and the typical pedestal ion energies are below the potential energies in the range of 400-800eV for the presented discharges and thus may explain the observed ELM power load asymmetries. Attributing the ELM power load asymmetry to a net asymmetry of ions arriving at the inner target plates, as conjectured in [2], the comparison of LP and IR gives numbers for the required ion temperatures of around 300 eV to match the heat fluxes calculated by both diagnostics [3].

Studies using the kinetic PIC code BIT1 [6] report that about 72% of the ELM deposited energy is carried by ions and $> 95\%$ of the fraction carried by electrons is also deposited on the time scale given by the ion sound speed $C_s = \sqrt{2T_{ion}/m_{ion}}$ assuming $T_{ion} \approx T_{electron}$. Thus, more than 98% of the ELM deposited energy arrives at the target plates with the typical time scale of $\tau_{||} = L_{||}/C_s$ [6] with $L_{||}$ being the SOL connection length.

In order to verify these recent results the paper presents detailed experimental analysis of the temporal power evolution on the inner/outer target plates with both field directions, focusing on the deposition time scales. Experimental details of the magnetic configurations, discharge parameters and diagnostic can be found in [3,7].

Temporal evolution of ELM power loading

As stated above, PIC-modelling [6] reports that basically the full fraction of energy is carried to the divertor on the ion time scale. A simple single particle expression may be used to approximate the power deposition at the inner (P_i) and outer (P_o) target plate. This function (see Eqn. (4.10) in [8] for details) describes the arrival of energy at the divertor target plates due to a Maxwellian distribution of collisionless particles (e.g. ions with temperature T_{ion}) released in the midplane to the SOL region:

$$P_{i,o}(t) = \frac{P_{i,o}^{max}}{0.84} \times \left(\frac{\tau_{i,o}}{t}\right)^2 \times \left(1 + \left(\frac{\tau_{i,o}}{t}\right)^2\right) \times \exp\left(-\frac{\tau_{i,o}}{t}\right)^2 \quad (1)$$

with $P_{i,o}^{max}$ being the maximum power deposition values and $\tau_{i,o}$ the ELM deposition time for the inner and outer target, respectively. Note that the maximum power load in this approximation is simply given by $P_{i,o}^{max} = P_{i,o}(t = 0.79 \cdot \tau_{i,o})$ [8]. The ELM power deposition time is expressed using the ion sound speed C_s and the ELM instability time τ_{ELM} by $\tau_i = L_{inner}/C_s + \tau_{ELM}$ and $\tau_o = L_{outer}/C_s + \tau_{ELM}$.

In Fig.1 experimental values of the inboard/outboard power deposition during an (coherent averaged) ELM are presented together with the fitted target power deposition function (Eqn.1) for (a) reversed and (b) normal field direction. Both, the inner and outer power deposition data, are fitted by one expression with five fit parameters $P_i^{max}, P_o^{max}, l = L_{outer}/L_{inner}, \tau_{ELM}$ and C_s. The connection length from inner to outer target is assumed to be $L_{||} = L_{inner} + L_{outer} = 2\pi R q_{95} = 51m$ with $R = 2m$ and $q_{95} = 4.3$. For convenience the results are presented in terms of T_{ion}. The agreement between experimental data and the (least square) fit is surprisingly good. Fig.1 also shows the ELM instability time (τ_{ELM}), the ion temperature (T_{ion}) and a measure for the poloidal location of the ELM energy release (L_{outer}/L_{inner}). The maximum power flux amplitudes for each target are not shown since they are obvious from the plot. Furthermore the time scales $\tau_{i,o}$, $\tau_{IR,i,o}$ and $\tau_{||,ped}$ are presented. The latter value, $\tau_{||,ped}$, takes the pedestal top (electron) temperature into account and was used for comparison to τ_{IR} for a variety of devices [9]. Results obtained here are in agreement to the results presented in [9].

Additionally 4 parameters describing the background correction are presented, which is performed before the data are fitted. The background before an ELM is assumed to be constant. The power load values for a time range of about 1ms before the ELM onset ($t_{ELM} = 0$) are averaged giving the parameters $P_{bef.,i}$ for the inner power load and $P_{bef.,o}$ for the outer target. As it can be seen in Fig.1, the minimum power deposition values in the tail of the ELM, $P_{tail,i}$, $P_{tail,o}$ tend to be slightly lower than $P_{bef.,i}$, $P_{bef.,o}$, respectively. This behaviour is commonly observed particular for the inner divertor and is explained by the reduced heat flux following an

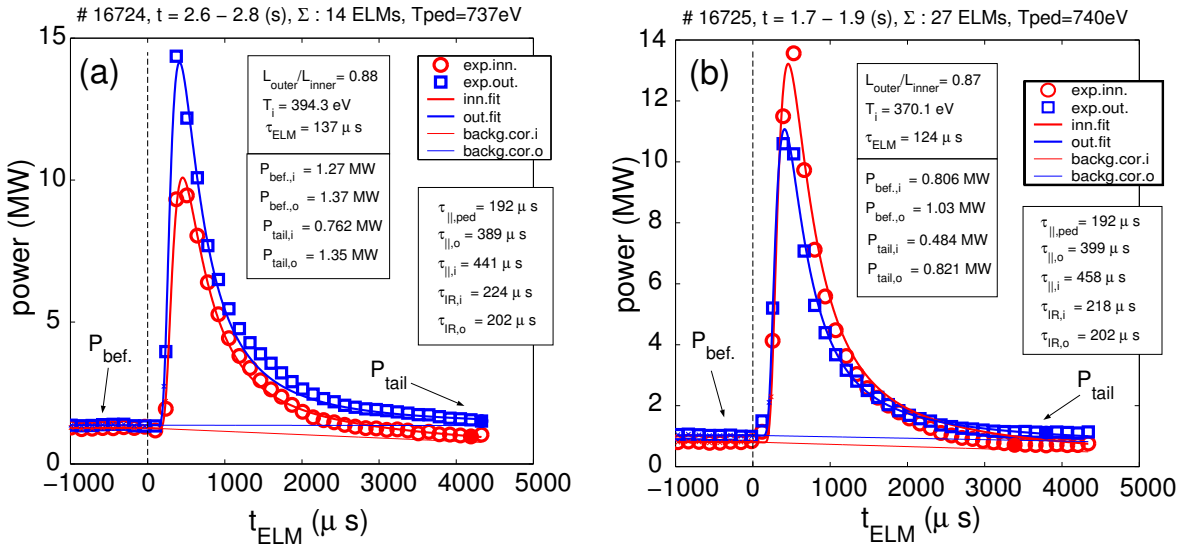

Figure 1: Experimental data of ELM power deposition, fitting curve and the background correction for type-I ELMy H-Mode with (a) reversed field and (b) normal field.

ELM compared to the before ELM time since after the ELM crash the pedestal energy recovers and the power crossing the separatrix is reduced. Therefore the background right after the ELM onset is assumed to be linearly decreasing down to a value between one and half of the before ELM background value, $0.5 \leq P_{tail,i,o}/P_{bef.i,o} \leq 1$. The changes of the fit parameters by varying $P_{tail,i,o}$ stay moderate as shown in Fig.2(a) for the data set presented in Fig.1(a). However, the choice of the exact value is performed in such a way that the resulting fit is best. The actual applied values for the background correction are presented in Fig.1.

Fig.2 (b) compares for a variety of USN discharges the fitting parameters for τ_{ELM}, T_{ion} and L_{outer}/L_{inner} to the electron pedestal top temperature measured by Thomson-Scattering in ASDEX Upgrade. All discharges presented here (and usually all in USN geometry in ASDEX Upgrade) have low densities when compared to high density / high confinement H-Modes plasmas. This has the beneficial aspect for diagnostics that both divertor legs stay power attached. Due to the absence of large gas puffing rates the ELM frequencies stay low and the released energy per ELM is comparable large for ASDEX Upgrade in the range between 20-30kJ. Also, the background correction appears to be less important since the ELM amplitudes are much larger than the background signal, whereas for high density cases and smaller ELMs the ELM peak heat fluxes are only moderately larger than the Inter-ELM heat fluxes.

Conclusions and Outlook

The main result of this work is that the ELM power deposition on the divertor target plates can be well described with a simple expression. Although the asymmetry of the integrated energy deposited energy as well as the maximum power deposition values P_i and P_o strictly change with the field direction [2], the temporal evolution does not show any significant differences between cases with normal and reversed field. The ELM instability time,τ_{ELM}, is found to be between 100-150μs. This value appears to be in a reasonable range. However, since τ_{ELM} enters the model in a rather ad-hoc manner, no further conclusions are drawn. The ion temperatures to explain the observed time scales for SOL transport vary around values of 400eV and are roughly consistent with (the comparison of) LP and IR data for ELMs for the lower divertor

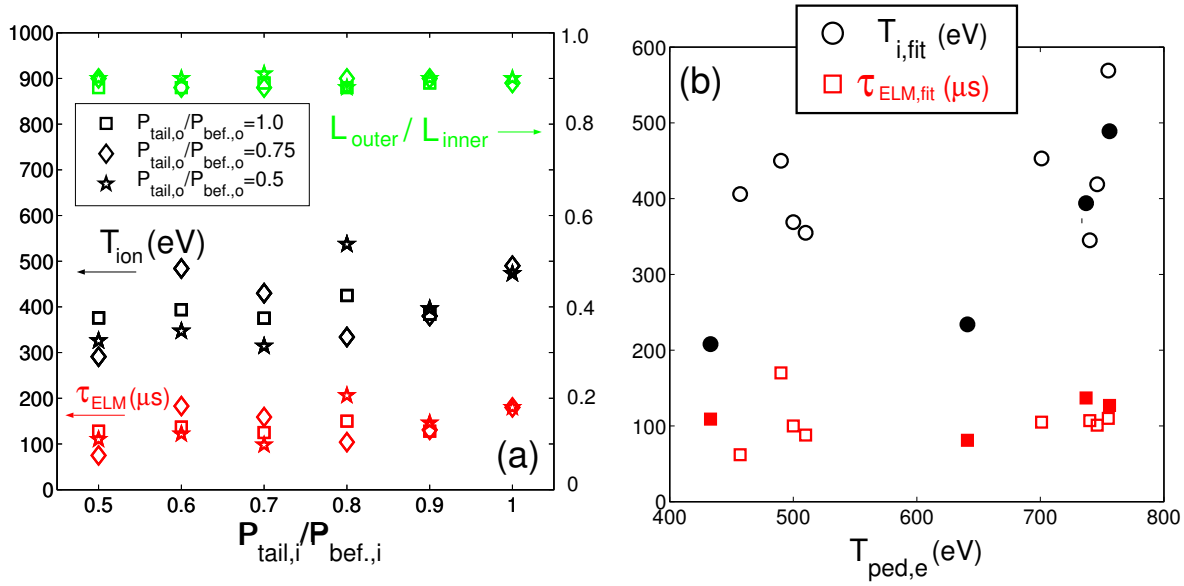

Figure 2: (a) Dependency of fit results on background correction for #16724. (b) Comparison of fit parameters (normal field open symbols, reversed field closed symbols) for a variety of discharges with different electron pedestal top temperatures.

[3] as well as with the picture of direct ion orbit losses. By attributing the target deposited energy of $2kT_{ion}/e$ to the orbit loss ions and taking the measured ELM energy/charge imbalance of 1kJ/1As (see Eqn.(1) in [2]) into account, values of $T_{ion} = 500eV$ are found. The resulting values for L_{outer}/L_{inner} of about 0.88 may surprise since it is commonly believed that due to its ballooning like nature the ELM energy transport is concentrated in the outer equatorial midplane. Moreover, basically no variation of this number has been found for all analysed data. However, different possibilities can be named to explain the observed values. First, the ELM energy release is indeed located in average above the equatorial midplane. Second, the numbers do not correctly describe the ELM energy release location but are due to the simplified description of the non-linear (and unknown) ELM energy release evolution. Finally, if first ion orbit losses play a significant role, the average temperature of ions deposited on the target receiving the higher energy load is expected to be higher there and thus different sound speeds for the inner and outer divertor power deposition have to be taken into account. To resolve this feature, modelling of first ion orbit losses during ELMs in ASDEX Upgrade is envisaged [10].

References

[1] A. Loarte et al., Plasma Physics Contr.Fusion **45** (2003) p.1549

[2] T. Eich et al., J. Nucl. Mat. **363-365**, 989 (2007).

[3] A. Kallenbach et al., this conference

[4] S.H. Hahn et al., Phys. Plasmas **12** (2005) 102501.

[5] J. Schirmer et al., Nuclear Fusion **46** (2006) S780-S791

[6] D. Tskhakaja et al., this conference

[7] T. Eich et al., Plasma Physics Contr.Fusion **47** (2005) p.815

[8] W. Fundamenski et al., Plasma Physics Contr.Fusion **48** (2006) p. 109

[9] T. Eich et al., J. Nucl. Mat. **337-339**, p.669-676 (2005).

[10] C.S. Chang et al., Phys. Plasmas **11** (2004) 2649.